Journal of Alloys and Compounds 499 (2010) 23–29

Contents lists available at ScienceDirect

Journal of Alloys and Compounds

journal homepage: www.elsevier.com/locate/jallcom

Magnetic properties of Fe–Co ferromagnetic layers and Fe–Mn/Fe–Co bilayers obtained by thermo-ionic vacuum arc

V. Kuncser[a,*], G. Schinteie[a], P. Palade[a], I. Jepu[b], I. Mustata[b], C.P. Lungu[b], F. Miculescu[c], G. Filoti[a]

[a] National Institute of Materials Physics, PO Box MG 7, 077125, Magurele-Bucharest, Romania
[b] National Institute for Lasers, Plasma and Radiation Physics, PO Box MG 36, 77125, Magurele-Bucharest, Romania
[c] "Politehnica" University, Bucharest, 06004, Romania

ARTICLE INFO

Article history:
Received 15 January 2010
Received in revised form 11 March 2010
Accepted 12 March 2010
Available online 18 March 2010

Keywords:
Magnetic films and multi-layers
Exchange coupling
MOKE
TVA

ABSTRACT

Simple Fe–Co ferromagnetic films and Fe–Mn antiferromagnetic films of different compositions were grown on epitaxial Si substrates with Ta buffer layers via thermo-ionic vacuum arc method. Fe–Co/Fe–Mn bilayer structures were obtained by following similar growing conditions as for the simple films. The magnetic behavior concerning easy axis distribution, anisotropy energy and coercive field of the Fe–Co films exchange coupled to the antiferromagnetic layers were discussed with respect to the magnetic behavior of the simple, uncoupled, ferromagnetic films. The composition of the antiferromagnetic films has a sensible influence on the magnetic parameters of the exchange coupled ferromagnetic films. The largest coupling and the narrowest easy axis distribution are induced in the bilayer system with equatomic composition of the Fe–Mn antiferromagnetic layer.

1. Introduction

Since the discovery of the exchange bias effect more than 50 years ago, by Meiklejohn and Bean [1], a new and exciting branch of modern magnetism has been rapidly grown up. The origin of the exchange bias effect is related to the interfacial exchange coupling of a thin ferromagnetic (F) layer sharing a common interface with an appropriate antiferromagnetic (AF) layer. The exchange coupling leads either to a shift of the hysteresis loop of the F layer with respect to the direction of the applied field, when an unidirectional anisotropy energy is involved at the interface (the shift is called exchange bias field) or to an increased coercivity, when only a common uniaxial anisotropy energy is involved. Clearly, both features lead to a different magnetization reversal of the F layer interfacially pinned to the AF layer, as compared with the case of a free F layer. Therefore, new spin valve devices were developed on basis of giant magneto-resistance (GMR)/tunneling magneto-resistance (TMR) effects generated in conductive/insulator thin films sandwiched between free and pinned F layers [2–4]. The equatomic composition of Fe–Mn was used for long time as a convenient AF layer and $Fe_{20}Ni_{80}$ (permalloy) as a suitable low coercive F layer in exchange biased spin valves [3,5]. In the state of art spin valve devices, Ir–Mn has replaced Fe–Mn due to enhanced intrinsic magnetic properties (e.g. higher Néel temperature as well as exchange anisotropy energy) and Co–Fe has replaced Ni–Fe due to a decreased atomic inter-diffusion at the F/Cu(conductive layer) interface. However, to optimize Fe–Mn as a valuable AF layer in AF/F bilayers for particular applications could become more convenient with respect to lower fabrication costs. This paper promotes a detailed study of the interfacial coupling in Fe–Mn/Fe–Co bilayer systems of different Fe concentrations in the Fe–Mn coupling layer, taking the advantage of the combinatorial processing procedure of the thermo-ionic vacuum arc method [6,7]. The orientation dependence of the anisotropy energy and coercive fields in the bilayer systems were compared and discussed with respect to the equivalent parameters of the free Fe–Co thin films.

2. Experimental

Simple ferromagnetic Fe–Co and antiferromagnetic Fe–Mn thin films as well as Fe–Mn/Fe–Co bilayers were deposited by thermo-ionic vacuum arc method on Ta buffer layers grown on (1 0 0) Si plackets (Ta thin films were also top deposited as protective cap layers). The currently used experimental arrangement of the thermo-ionic vacuum arc method, involves two electron beams generated by heated cathodes and accelerated by high anodic voltages. The materials, placed in special crucibles at the anodes, are evaporated via electron bombardment. The evaporating species, metals and alloys in our case, can be deposited on a series of substrates, located at different distances from the anode positions. The experimental arrangement using four different crucibles at each of the two anodes (the crucibles are rotating in the same anodic position via a special device) allows either the simultaneous deposition from two different crucibles or the simple deposition from only one crucible. However, using this design, each different substrate can be indexed by only one (in case of one source deposition) or two (in case of two sources deposition) distances from the anodic positions. Hence, a two sources deposition leads to a combinatorial preparation of thin film alloys of different concentrations, depending on the position of the substrate with respect to the two anodic positions where

* Corresponding author. Tel.: +40 21 369 01 85; fax: +40 21 369 01 77.
E-mail address: kuncser@infim.ro (V. Kuncser).

0925-8388/$ – see front matter © 2010 Elsevier B.V. All rights reserved.
doi:10.1016/j.jallcom.2010.03.129

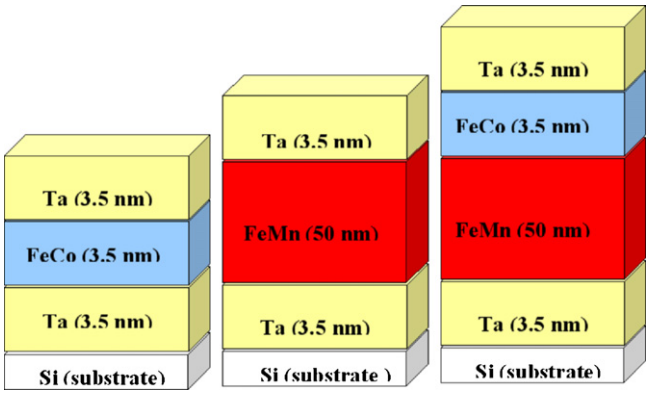

Fig. 1. The geometrical structure of the analysed samples, as follows: (a) set F_*n*, (b) set AF_*n* and (c) set AF/F_*n*.

the evaporating materials are placed. Let us note the distance from anode 1 by d_{A1} and the distance from anode 2 by d_{A2}. Four substrate positions (1, 2, 3, and 4) have been considered for each preparation, involving the following couple of distances d_{A1}/d_{A2} (in mm): 160/200, 185/175, 200/165 and 215/155, for the mentioned positions, respectively. The three prepared sets of samples are presented in Fig. 1. A Fe–Co alloy closed to the equatomic composition was previously prepared by arc-melting and introduced in one of the four crucibles at anode 1. Similarly, Ta foils were introduced in a crucible at anode 2. In conditions of one source evaporation, almost similar Fe–Co relative contents are expected for the thin films grown on all the four substrates placed at positions 1–4, but also a diminushed thickness of the Fe–Co thin films when moving from position 1 to 4 (and similarly a higher thickness of the Ta films, when moving in the same sense). It is worth mentioning that the generic thicknesses given in Fig. 1, correspond to average thicknesses per preparation, measured by only one quartz balance (Kressington) placed between positions 2 and 3. For preparing the Fe–Mn thin films, a two sources preparation procedure was used, by inserting Fe in a crucible at anode 1 and Mn in a crucible at anode 2 and initiating a simultaneous deposition. Due to the experimental design, Fe–Mn thin films with increasing Mn content when moving from position 1 to 4 of the substrates are expected. The relative variation of the thickness of the Fe–Mn films has to be this time almost insignificant, due to the much higher thickness of the film (more than one order of magnitude thicker than in the case of the Fe–Co film) on one hand and, on the other hand, to the simultaneous evaporation with almost similar rates from both sources at anode 1 and 2. Finally, in case of the bilayer system, the preparation was done with materials inserted in crucible exactly as above mentioned for the simple films and following the same evaporation procedure. Therefore, the thicknesses and composition of each of the two films in the bilayer structure belonging to one position of the substrate, have to be identical with the ones in single films corresponding to the same substrate position. However, a different magnetic texture would be expected for the Fe–Co thin films grown on Fe–Mn layers of different Fe relative content, as compared with the films grown on the Ta buffer. The interfacial coupling can also modify the coercive force and the shift of the hysteresis loop in the exchange coupled Fe–Co films. Therefore, the magnetic behavior of the Fe–Co layers exchange coupled to Fe–Mn layers of different relative concentrations has been analysed essentially with respect to the behavior of the corresponding free (uncoupled), Fe–Co layers. The prepared samples were labeled as follows (see also Fig. 1): (a) F_*n* with $n = 1, 2, 3, 4$ indexing the substrate position, for simple ferromagnetic Fe–Co films with Ta both as buffer and cap layer, (b) AF_*n* for simple antiferromagnetic Fe–Mn films with Ta deposited as buffer and cap layer and (c) AF/F_*n*, for Fe–Mn/Fe–Co bilayer systems with Ta again as buffer and cap layer. The relative content of Fe in the AF_*n* films as well as in the F_*n* films was estimated by Energy Dispersive X-ray (EDX) technique and the film surface quality was checked by Scanning Electron Microscopy. The room temperature magnetic reversal processes in the free as well as in the coupled Fe–Co films were characterized by longitudinal magneto-optic Kerr effect (MOKE). A MOKE device (type AMACC) working in longitudinal geometry and using a magnet with laminated sheets with essentially zero remanence and negligible hysteresis was utilized. The device is provided with a step motor for rotating the sample in its own plane, with a precision better than 0.5°. The wavelength of the incident light, provided by a laser diode, is about 640 nm. The angle of incidence is 45° and the incident light is linearly polarized along the sample plane. A brief low temperature characterization of the magnetization reversal at 5 K was performed via VSM magnetometry, in a close cycle Cryogenics cryomagnet. All the magnetic measurements were performed on square-shaped samples, with an area of about 81 mm^2 for MOKE measurements and of about 10 mm^2 for VSM measurements and with the magnetic field applied along the sample plane. The cutting edge of the sample with respect to the crystallographic axis of the Si substrate was validated by X-ray diffraction.

3. Results and discussions

The relative content of Fe and Co in the 2 extremities samples F_1 and F_4, as determined by EDX, was 50–50 at.% in sample F_1 and 52–48 at.% in sample F_4, respectively. Within the error limits of 1–2 at.%, we may consider that all the F_*n* films present the same composition, close to the equatomic ratio. This consideration is also in agreement with the preparation procedure based on the evaporation of an Fe–Co alloy from only one evaporation source. However, the ratio between the relative wt.% of Fe–Co and of the Ta decreases from 1.5 in sample F1 down to 0.7 in sample F_2, proving clearly a decreased thickness of the Fe–Co film and an increased thickness of the Ta buffer, when moving from position 1 (closer to anode 1, where the Fe–Co crucible was placed) to position 4 (closer to anode 2, where the Ta crucible was placed). Roughly, from the wt.% EDX delivered data, the thickness of the Fe–Co film in sample F_4 was estimated at about 0.7 from the thickness of the ferromagnetic film in sample F_1. Starting from the indication of the quartz balance placed between positions 2 and 3, it can be inferred that the thickness of the Fe–Co films decreases from about 4 nm for F_1 down to 3 nm for F_4. The magnetization reversal in samples F_1 and F_4 was analysed by longitudinal MOKE, at different orientations of the Si substrate edge, with respect to the direction of the applied magnetic field. X-ray diffraction scans were performed on Ta grown on the Si substrate, with the radiation incident on the sample plane at a fix small angle and moving only the detector in the incidence plane from 15° to 60°. With the edge of the sample along the radiation beam, only the 3 1 1 diffraction line of Si with face center cubic structure (fcc), space group $Fd\bar{3}m$, as well as 1 1 1 and 2 0 0 diffraction lines of Ta with fcc structure, space group $Fm\bar{3}m$, were observed. Rotating the sample by 45° in its own plane, the Si line disappeared completely whereas the two lines of Ta remained both present, just with a slightly diminished intensity ratio I_{111}/I_{200}. That proves clearly the edge of the mono-crystalline Si is cut along the [1 1 0] crystallographic direction and a poly-crystalline layer of Ta with a slight texture also along [1 1 0] is formed. The hysteresis loops of the F films with extreme thickness, F_1 and F_4, collected at three different orientations, $\theta = 0°$, 45° and 90° (where $\theta = 0°$ means that the sample edge, which is along the [1 1 0] axis of Si, is parallel to the applied field, whereas $\theta = 90°$ means that it is perpendicular to the applied field) are shown in Fig. 2(a) and (b) respectively. At a very first glance two important aspects can be mentioned from these results: (i) the hysteresis loops evolve with θ angle, from a more rectangular shape and higher coercivity at $\theta = 0°$ to an almost closed shape of much lower coercivity at $\theta = 90°$ and (ii) at $\theta = 0$, the hysteresis loop of sample F_4 is more rectangular than the hysteresis loop of sample F_1 whereas at $\theta = 90°$, sample F_4 show no coercivity as compared with the finite coercivity of sample F_1. These results can be qualitatively explained via the simple Stoner–Wolfarth model [8,9] of a ferromagnetic film (when a single domain state is considered) with in-plane uniaxial anisotropy. It is worth mentioning that Conversion Electrom Mossbauer spectra of the Fe–Co films enriched in the ^{57}Fe isotope have proven the in-plane spin orientation of the analysed films [10]. Defining K_F as the anisotropy constant, θ as the orientation of the applied field with respect to the anisotropy direction (easy axis of magnetization), M_F the saturation magnetization and β the orientation of the magnetization with respect to the anisotropy direction, the magnetic energy per unit volume of the ferromagnetic film is:

$$E = -\mu_0 H M_F \cos(\theta - \beta) + K_F \sin^2 \beta \quad (1)$$

where the first term represents the magnetic Zeeman contribution and the second one is the contribution of the magnetic anisotropy. Angle β is deduced from the condition of the minimization of the magnetic energy with respect to this angle, for each value and

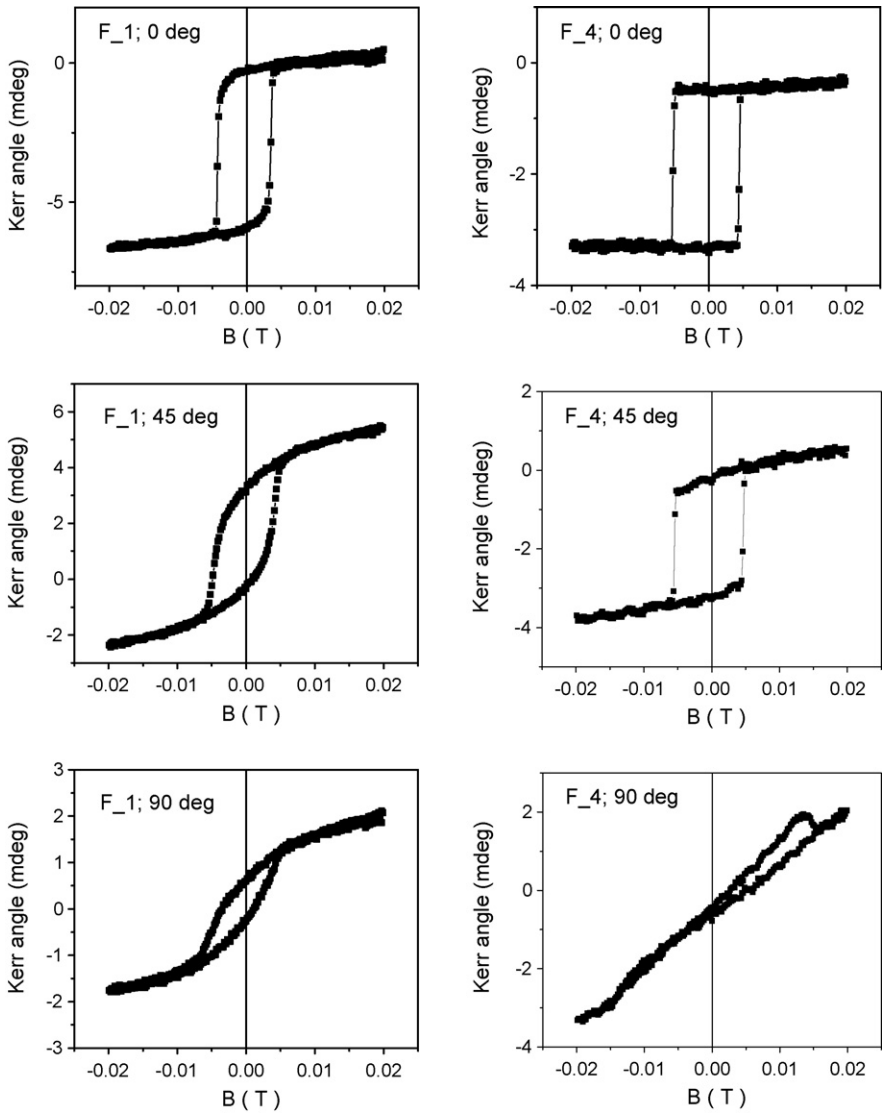

Fig. 2. Room temperature MOKE loops obtained on samples F_1 (a) and F_4 (b), for different orientations between the applied field and the average easy axis of magnetization.

orientation of the magnetic field with respect to the anisotropy direction. Hence, the longitudinal component of the magnetization, $m_{//} = \cos(\beta - \theta)$, which is exactly what has been measured by MOKE, can be computed for each value of the applied field, once the direction of the applied field versus the anisotropy direction is given. The obtained hysteresis loops evolve with angle θ, from a fully rectangular shape at $\theta = 0$, to a fully closed shape (linear dependence without coercivity) at $\theta = 90^\circ$ [9]. The results in Fig. 2 can be therefore interpreted in terms of the proposed approach. However, the model belongs to an ideal case, assuming a unique direction of anisotropy. An angular easy axis distribution has to be expected in real systems, depending on the magnetic texture of the system, leading finally to much curved loops in both the two extreme cases of $\theta = 0^\circ$ and 90°, respectively. Based on these considerations, it might be reasonable assumed, for the analysed systems, that: (i) all the F films show a magnetic texture with the easy axis oriented in average (e.g. the maximum of the angular easy axis distribution) along the [1 1 0] direction of the Si substrate and (ii) the specific magnetic texture is enhanced in the thinner F_4 film, as compared with the thicker F_1 film which shows a much broader angular easy axis distribution (EAD). Another feature of the Stoner–Wolfarth theory applied for systems of uniaxial anisotropy, is the dependence of the coercive field on the magnitude of the anisotropy constant, when the magnetic field is applied along the easy axis. In this case, of the most rectangular shape of the hysteresis loop (that is at $\theta = 0$ or equivalently, π), the coercive field becomes $H_c = 2K_F/\mu_0 M_F$. It is worth mentioning that absolute values of saturation magnetization are not accessible by MOKE experiments. In spite of the expected proportionality between the magnetization at saturation and $\Delta\theta_{Kerr}/2$, where $\Delta\theta_{Kerr}$ is the difference between the Kerr angle at saturation in positive and negative fields, the simple comparison of $\Delta\theta_{Kerr}$ becomes usefulness when comparing different samples with respect to their saturation magnetization, due to possible different light scattering amplitudes, dependent on the surface quality. Anyhow, based on physical reasons, it might be reasonable assumed that the magnetization at saturation in sample F_1 is similar to the one in sample F_4, due to the same film composition. Hence, the ratio of the anisotropy constants of samples F_1 and F_4 can be expressed as: $K_F^1/K_F^4 = H_C^1 M_F^1/H_C^4 M_F^4$. The coercive fields evidenced by the MOKE curves at $\theta = 0$ are $H_C^1 = 40$ Oe (sample F_1) and $H_C^4 = 50$ Oe (sample F_4). Roughly, the above relation gives a slightly higher anisotropy constant for sample F_4 as compared with sample F_1 (e.g. about 20% higher), which most probable is related to its lower thickness. Specifically, the F films have slightly different average anisotropy constants as well as different angular easy axis distributions.

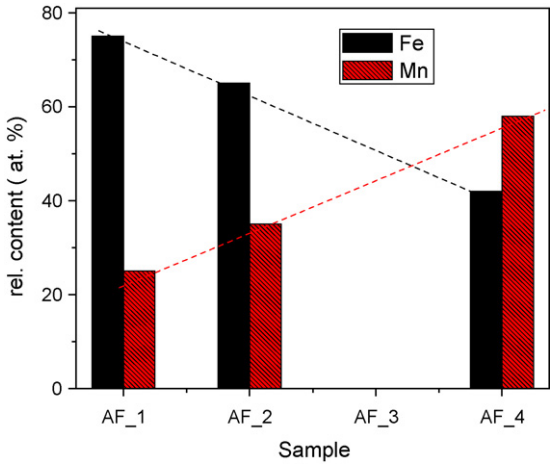

Fig. 3. The relative content of Fe and Mn in the AF films, as obtained by EDX analysis.

On the other side, one main interest was to analyse the changes induced in the magnetization reversal of similar ferromagnetic Fe–Co layers coupled to antiferromagnetic Fe–Mn layers with different Fe concentrations. For the estimation of the relative Fe (or Mn) content in the AF films, samples AF_1, 2 and 4 were characterized by EDX. The results, normalized to the Fe and Mn relative content (Ta is also present), are shown in Fig. 3. It is obvious that the relative content of Fe decreases almost linearly from about 70% in sample AF_1 down to about 40% in sample AF_4. Derived from these results, sample AF_3 should present an almost equiatomic composition of $Fe_{50}Mn_{50}$.

It is worth to mention that the magnetic phase diagram of fcc Fe_xMn_{100-x} alloys has been investigated over a large range of concentrations by Endoh and Isikawa [11] who found an antiferromagnetic long range order for $40\% < x < 80\%$, namely where the presently prepared compounds are placed. Neel temperatures lower than 295 K were mentioned in [12] for $60\% < x < 80\%$ and higher than 295 K for $40\% < x < 60\%$ (a maximum of about 500 K is reached for the equatomic composition). However, characteristics of the magnetic structure of Fe–Mn alloys are very sensitive also to the preparation conditions/techniques, and therefore, the presently involved AF films were verified by MOKE with respect to their AF structure at room temperature. None of the simple AF films prepared by TVA have presented MOKE signals typical to ferromagnetic or paramagnetic state over the field range from 500 Oe to −500 Oe, in spite of a thickness 14 times larger than for the F films, giving experimental support for antiferromagnetic order in all AF films at room temperature. Therefore, one may assume that in the AF/F_*n* samples, the magnetic signal belongs entirely to the pinned F layer. One should mention at this point that at about 640 nm, the refractive indices and the extinction coefficients of Ta, Fe, Co and Mn are about 1.7, 2.2, 2.8, 2.5 and 2.2, 3.0, 4.0, 3.6, respectively [13]. Hence, the following relation between the refractive indexes of the

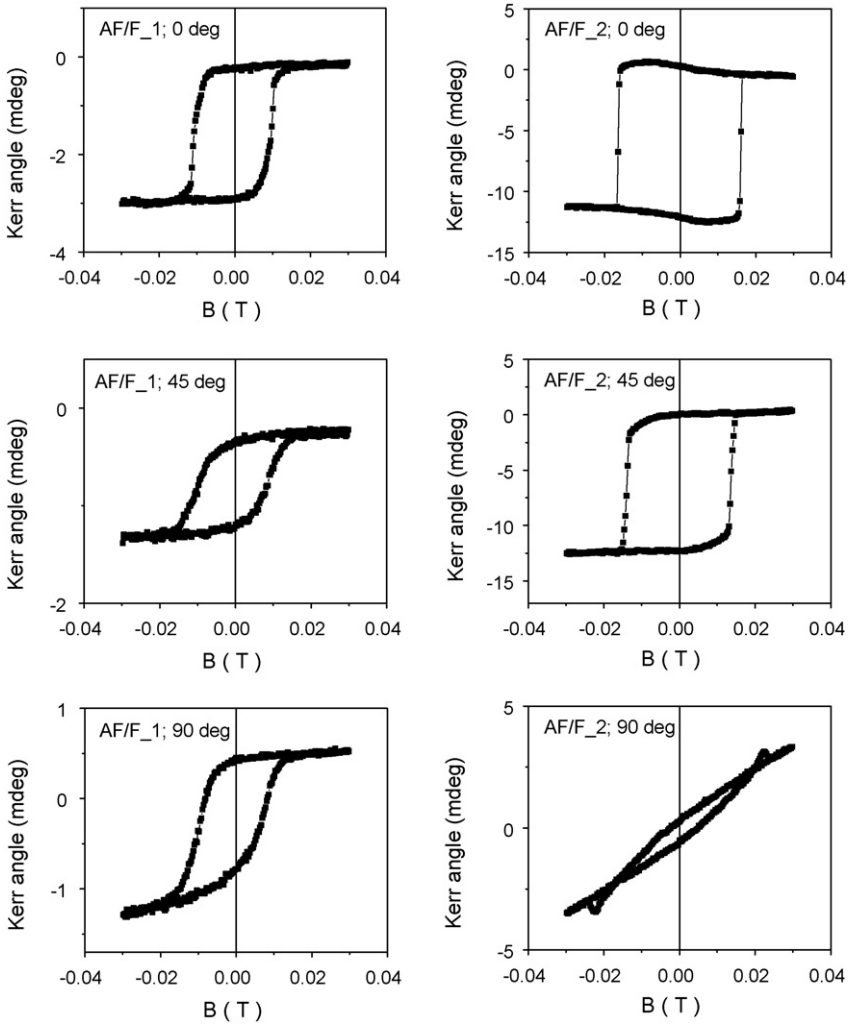

Fig. 4. Room temperature MOKE loops obtained on samples AF/F_1 (a) and AF/F_2 (b), at different angles θ.

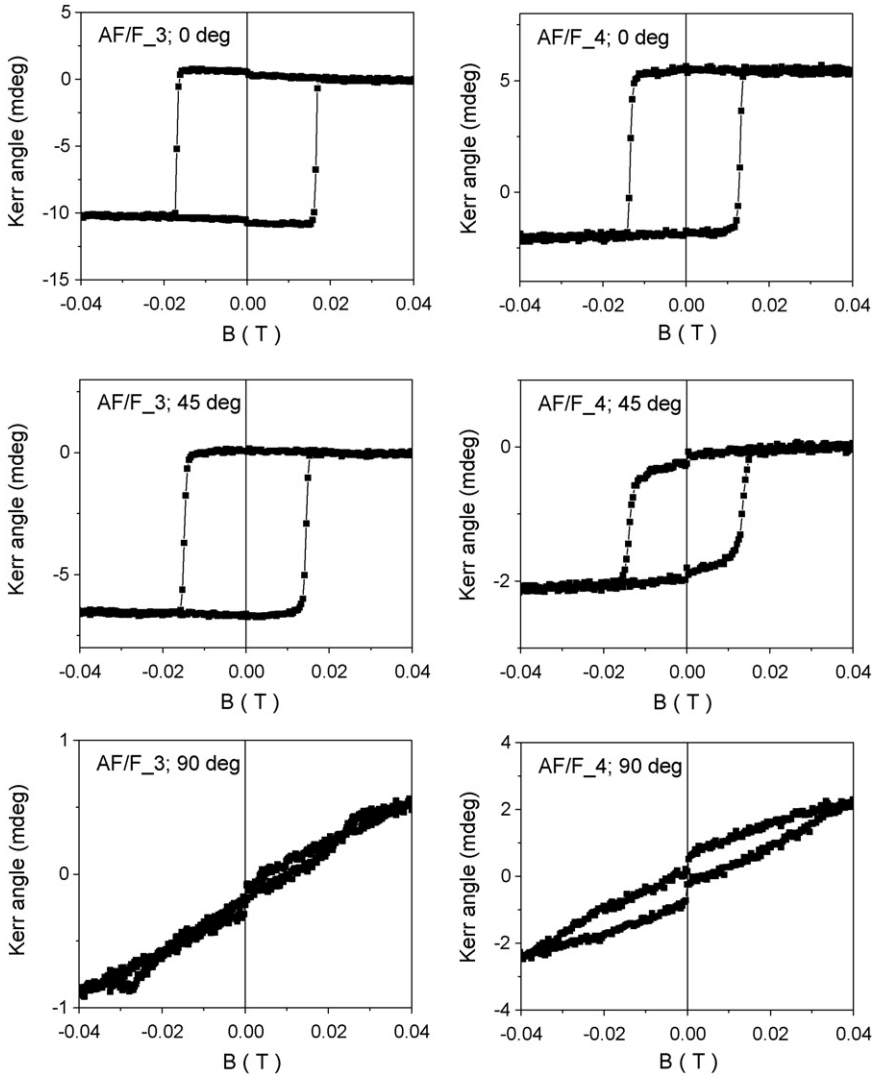

Fig. 5. Room temperature MOKE loops obtained on samples AF/F_3 (a) and AF/F_4 (b), at different angles θ.

different layers has to be considered: $n_{air} < n_{Ta} < n_{Fe-Mn} < n_{Fe-Co}$ (the refractive indices of the alloys were assumed as weighted average of the two involved elemental refractive indices). Taking into account the angle of incidence, the above mentioned refractive indices, the Snellius law and the typical expression of the reflection coefficient for the *s* component of the light at each metallic interface as well as the exponential attenuation of the incident beam in the layers [14], it can be roughly estimated that the light penetrate trough both the Ta/Fe–Co and Fe–Co/Fe–Mn interfaces (no total reflection condition is fulfilled at these interfaces). The intensity at the Fe–Co/Fe–Mn interface is only 20% from the initial one and only a few percents from the intensity reaching the detector belongs to the ferromagnetic layer. However, this amount is order of magnitudes larger than the component escaping back from the much thicker Fe–Mn layer, which anyhow does not show effective magnetization. The MOKE hysteresis loops of samples AF/F_1, 2 and AF/F_3, 4 are shown in Figs. 4 and 5, respectively. As in the case of the uncoupled F films, a similar trend of the loops features versus the θ angle is observed. However, the curving of the loops when moving from $\theta = 0$ to $\theta = 90^\circ$, as well as the coercive field values at $\theta = 0^\circ$, are strongly dependent on the composition of the AF pinning layer.

The results may be interpreted in the frame of simple Meiklejohn and Bean model [15,9], which is in fact a Stoner–Wohlfarth model which takes additionally into account the magnetocrystalline anisotropy of the antiferromagnet (K_{AF}) and the interfacial exchange coupling energy per unit area (J_{ex}) acting at the AF/F interface. Because of the exchange coupling energy is specific to the area unit, all the involved energies are transformed in energies per unit area by multiplying the corresponding energies per unit volume with the thickness of the involved films (t_F and t_{AF}, for the F and AF films, respectively). Accordingly, the magnetic energy per unit surface becomes:

$$E_S = -\mu_0 H M_F t_F \cos(\theta - \beta) + K_F t_F \sin^2 \beta + K_{AF} t_{AF} \sin^2 \alpha - J_{ex} \cos(\beta - \alpha) \quad (2)$$

with θ and β as previously mentioned and α the new angle between the net magnetization at the AF interface (required by any coupling effect) and the anisotropy direction of the AF layer. The same procedure of minimization of the magnetic energy with respect to angles α and β can be used for the evaluation of the hysteresis loops, but for a qualitative interpretation of the experimental data, only two limit cases will be further discussed. The first one corresponds to a much larger anisotropy energy of the AF phase with respect to the exchange coupling energy ($K_{AF} t_{AF} \gg J_{ex}$). In this case, the net magnetization of the AF film at the interface, M_{AF}, will remain always along the anisotropy direction during the reversal process of the F layer and hence, always $\alpha = 0$. No additional coer-

cive field is induced, but the loop is shifted by a maximum exchange bias field, defined as $H_{eb} = -J_{eb}/\mu_0 M_F t_F$. The second case corresponds to a much higher exchange coupling energy, with respect to the anisotropy energy of the AF phase ($K_{AF}t_{AF} \ll J_{ex}$). Accordingly, the net magnetization at the AF interface will follow always the magnetization of the F layer and hence $\alpha = \beta$. In this case, there is no shift of the loop ($H_{eb} = 0$) whereas the coercive field might be roughly expressed by: $H_c \approx (2K_F t_F + 2K_{AF}t_{AF})/\mu_0 M_F t_F$ (see relation (2) for $\alpha = \beta$). It is worth mentioning that for $K_F t_F \ll K_{AF}t_{AF}$ the above relation leads to a coercive field expressed by $H_c \approx 2K_{AF}t_{AF}/\mu_0 M_F t_F$, whereas for $K_F t_F \gg K_{AF}t_{AF}$, $H_c = 2K_F/\mu_0 M_F$, in agreement with the simple Stoner–Wohlfarth model. As observed in Figs. 4 and 5, the experimental loops of the AF/F bilayers can be framed via the lack of the exchange bias field and of the regular shape of the hysteresis loop, only to the case of exchange coupling energy much higher than the anisotropy energy of the AF film. In this case, the coercivity of the F layer coupled to the AF layer might be roughly approximated via the above relation, which consider the uniaxial anisotropy of the AF layer just adding to the uniaxial anisotropy energy of the ferromagnetic layer. Thus, most of the discussions involving simple F films remain valid for the AF/F systems, except the additional contribution of the uniaxial anisotropy, due to the AF phase.

Sample AF/F_1 starts with a more rounded loop already at $\theta = 0^\circ$ and ends up with a quite asymmetric and still round loop at $\theta = 90^\circ$ (see Fig. 4(a)), proving the presence of an angular easy axis distribution of consistent width. The angular EAD of the F films coupled to the AF layers is much narrow for the other three samples (rectangular loops at $\theta = 0^\circ$ and almost no open loop at $\theta = 90^\circ$), with a special mention for sample AF/F_3. However, none of these loops exhibit any shift with respect to the zero field (negative shifts below 10 Oe are due to the magnet remanence), indicating an exchange coupling energy higher than the anisotropy energy of the AF layer, as already discussed. The coercive fields at $\theta = 0$ are 100(3), 160(3), 170(3) and 135(3) Oe, for samples AF/F_1, 2, 3 and 4, respectively. A simple comparison with coercive fields of 40–50 Oe, as pointed out for the free F films, stands clearly for an enhanced uniaxial interfacial coupling in the F films coupled to the AF layers. Granting an almost similar magnetization at saturation for the simple F film as well as for the AF/F film corresponding to the same position, double and even triple coercive fields observed in the AF/F bilayers means additional contributions from the uniaxial anisotropy energy of the AF layer, equal or doubles than the contribution of the F layer. Corroborating with the already stated condition, $K_{AF}t_{AF} \ll J_{ex}$, it results exchange coupling energies equal or higher than the anisotropy energy of the F layer. The highest exchange coupling energy as well as exchange anisotropy, corresponds to sample AF/F_3 with equatomic composition of the AF film, showing the highest coercive field.

Finally, one aspect which has to be briefly mentioned, concerns temperature effects related to the different anisotropy energies in such systems. In this view, the two hystersis loops obtained at 5 K via vibrating sample magnetometry, on samples F_4 and AF/F_4, respectively, are shown in Fig. 6. In both cases the field was applied along the sample plane, oriented at $\theta = 45^\circ$ versus the sample edge, that is at 45° versus the easy axis. It is worth mentioning that the room temperature MOKE data have evidenced for this field orientation, quite round loops for both samples (see Fig. 2(b) and Fig. 5(b)), corresponding well to the intermediate case between rectangular (at $\theta = 0^\circ$) and linear (at $\theta = 90^\circ$) shapes of the Stoner–Wohlfarth model. Surprisingly, the magnetization reversal process in sample F_4 follows a quasy-linear dependence, inferring a rotation of the magnetization easy axis by 45° (perpendicular to the applied field) at low temperature. On the other hand, the hysteresis loop of the coupled films (sample AF/F_4), keeps a more rounded shape and appears as shifted sensibly to a negative field, proving undoubtedly

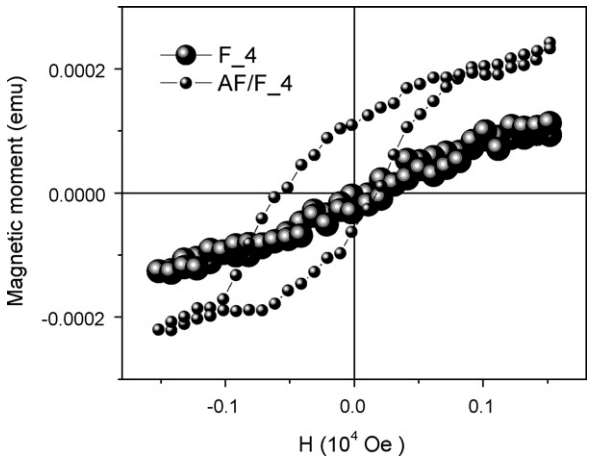

Fig. 6. VSM hysteresis loops obtained at 5 K on samples F_4 and AF/F_4. The applied longitudinal field was oriented at $\theta = 45^\circ$ with respect to [1 1 0] direction of Si.

the presence of the unidirectional anisotropy at low temperature. The coercive field at 5 K is 390 Oe (135 Oe at room temperature) whereas the exchange bias is −200 Oe (neglijible at room temperature). Therefore, the lack of the exchange bias field at room temperature has to be connected with magnetic relaxation phenomena leading to a low blocking temperature, most probable due to the decreased anisotropy energy of the AF phase.

4. Conclusions

Three layered systems consisting of simple F ($Fe_{50}Co_{50}$) and AF (Fe_xMn_{100-x}) films, as well as of exchange coupled AF/F layers have been successfully prepared by thermo-ionic vacuum arc method. The Fe–Mn relative content in the AF films was varied from 75–25 at.% to 45–55 at.% by positioning the epitaxial Si substrates at different distances from the Fe and respectively Mn sources. Buffer and cap layers of Ta were used in all situations. Simple F films present a magnetic texture with an average orientation of the easy axis (the maximum of the angular EAD) along the [1 1 0] direction of Si. The average uniaxial anisotropy constant is slightly increasing for thinner simple F films. Also a narrower width of the angular EAD was evidenced for thinner F films, obtained by fixing the Si substrates more far away from the Fe–Co source. The directly observed angular EAD in the AF/F systems belongs strictly to the F films, but its intimate origin is related also to the interfacial exchange coupling to the AF layer. Both the width of the EAD as well as the coercive field of the F layer coupled to the AF layer depends on the relative composition of the Fe–Mn AF film. The broadest EAD corresponds to the system with 75 at.% of Fe in the AF layer. The largest pinning of the F layer was observed for the equiatomic composition of the AF layer. The observed lack of unidirectional anisotropy at room temperature implies that exchange coupling energy is larger than the uniaxial anisotropy energy of the aniferromagnetic layer, in all the analysed systems. The unidirectional anisotropy appears in the AF/F bilayer systems at low temperatures. A rotation of the magnetic easy axis in the simple F systems was also observed at low temperature.

Acknowledgement

The financial support through the Romanian National project PNII-71-032 is highly acknowledged.

References

[1] W.H. Meiklejohn, C.P. Bean, Phys. Rev. 102 (1956) 1413–1414.

[2] S.A. Wolf, S.D. Treger, A. Chtchelkanova, MRS Bull. 31 (2006) 400–403.
[3] M. Johnson, Magnetoelectronics, Elsevier, Amsterdam, 2004 (Chapters 2 and 3).
[4] S. Parkin, MRS Bull. 31 (2006) 389–393.
[5] J.M.D. Coey, in: M.J. Thornton, M. Ziese (Eds.), Materials for Spin Electronics. LPN, vol. 569, Springer-Verlang, Berlin Heidelberg, 2001, pp. 277–297.
[6] I. Mustata, C.P. Lungu, A.M. Lungu, V. Zaroski, M. Blideran, V. Ciupina, Vacuum 76 (2004) 131–134.
[7] C.P. Lungu, I. Mustata, G. Musa, A.M. Lungu, V. Zaroschi, K. Iwasaki, R. Tanaka, Y. Matsumura, I. Iwanaga, H. Tanaka, T. Oi, K. Fujita, Surf. Coat. Technol. 200 (2005) 399–402.
[8] E.C. Stoner, E.P. Wohlfarth, Nature 160 (1947) 650.
[9] F. Radu, H. Zabel, Springer Tracts Modern Phys. 227 (2007) 97–184.
[10] V. Kuncser, G. Schinteie, P. Palade, I. Jepu, O. Pompilian, I. Mustata, C.P. Lungu, F. Minculescu, G. Filoti, in press.
[11] Y. Endoh, Y. Ishikawa, J. Phys. Soc. Jpn. 30 (1971) 1614–1627.
[12] T. Anhoj, C.S. Jacobsen, S. Morup, J. Appl. Phys. 95 (7) (2004) 3649.
[13] E.D. Palik, Handbook of Optical Constants of Solids, Academic Press, Boston, 1991 (see also http://refractiveindex.info).
[14] M. Mansuripur, The Physical Principles of Magneto-optical Recording, Cambridge University Press, 1995, pp. 128–163.
[15] W.H. Meiklejohn, C.P. Bean, Phys. Rev. 105 (1957) 904–913.